Available online at www.sciencedirect.com
ScienceDirect
Icarus 191 (2007) 636–650
ICARUS
www.elsevier.com/locate/icarus

Generalized YORP evolution: Onset of tumbling and new asymptotic states

D. Vokrouhlický [a,*,1], S. Breiter [b], D. Nesvorný [a], W.F. Bottke [a]

[a] *Southwest Research Institute, 1050 Walnut St, Suite 400, Boulder, CO 80302, USA*
[b] *Astronomical Observatory, Adam Mickiewicz University, ul. Słoneczna 36, PL 60-286 Poznań, Poland*

Received 1 March 2007; revised 31 May 2007

Available online 4 July 2007

Abstract

Asteroids have a wide range of rotation states. While the majority spin a few times to several times each day in principal axis rotation, a small number spin so slowly that they have somehow managed to enter into a tumbling rotation state. Here we investigate whether the Yarkovsky–Radzievskii–O'Keefe–Paddack (YORP) thermal radiation effect could have produced these unusual spin states. To do this, we developed a Lie–Poisson integrator of the orbital and rotational motion of a model asteroid. Solar torques, YORP, and internal energy dissipation were included in our model. Using this code, we found that YORP can no longer drive the spin rates of bodies toward values infinitely close to zero. Instead, bodies losing too much rotation angular momentum fall into chaotic tumbling rotation states where the spin axis wanders randomly for some interval of time. Eventually, our model asteroids reach rotation states that approach regular motion of the spin axis in the body frame. An analytical model designed to describe this behavior does a good job of predicting how and when the onset of tumbling motion should take place. The question of whether a given asteroid will fall into a tumbling rotation state depends on the efficiency of its internal energy dissipation and on the precise way YORP modifies the spin rates of small bodies.

Keywords: Rotational dynamics; Asteroids, rotation

1. Introduction

There has been a rapid increase over the last 10 years in the quantity of asteroid rotation rate data obtained from lightcurve observations (e.g., Pravec et al., 2007) and radar (Ostro et al., 2002). Yet another order of magnitude increase is expected when photometrically-calibrated sky surveys such as Pan-STARRS come on-line (e.g., Ďurech et al., 2007). As new telescopes become available for asteroid studies, the population of objects with known rotation state will begin to extend to smaller objects. If experience is any guide, this data will present us with numerous unexplained problems; previous examples include the collinearity of spin vectors found among prograde-rotating Koronis family members (e.g., Slivan, 2002; Slivan et al., 2003) and the strongly non-Maxwellian distribution of rotation rates seen among small ($D \lesssim 10$ km) asteroids (e.g., Pravec et al., 2007). The challenge is to expand existing asteroid rotation evolution theory prior to these advances taking place.

Prior to the last several years, the effects of torques produced by incident radiation from the Sun or a planet were used to understand the attitude of artificial satellites (e.g., Burns et al., 1979, or references in Rubincam, 2000). In recent years, however, the interest of these torques on small asteroids and meteoroids has increased, perhaps due to successful applications of related radiative forces in the orbital motion of planetary bodies. The effects of the thermal component of these radiative torques, which are due to infrared emission of absorbed sunlight from the surface of a body, was first described and characterized by Rubincam (2000). Rubincam coined an acronym for these torques called YORP, which stands for Yarkovsky–O'Keefe–Radzievskii–Paddack (after several researches who pioneered the study of radiative torques in the 1950s and 1960s). Rubincam (2000) showed that YORP torques can produce pronounced secular changes in the

* Corresponding author.
E-mail address: vokrouhl@cesnet.cz (D. Vokrouhlický).
[1] On leave from Institute of Astronomy, Charles University, V Holešovičkách 2, 18000 Prague 8, Czech Republic.

0019-1035/$ – see front matter
doi:10.1016/j.icarus.2007.06.002

spin vectors (i.e., rotation rates and obliquities) of small asteroids and meteoroids.

Since that classical paper, YORP torques have been used to explain why (i) the spin vectors of Koronis family members are aligned (Vokrouhlický et al., 2003), (ii) small objects in asteroid families tend to have semimajor axes near the periphery of the family (Vokrouhlický et al., 2006a, 2006b) and (iii) some multi-km asteroids have escaped the main belt (in conjunction with the Yarkovsky effect and resonances) and are now in the planet-crossing region (Morbidelli and Vokrouhlický, 2003). Moreover, precise photometry and radar observations have allowed us to directly detect the effects of YORP on two near-Earth asteroids: (54509) 2000 PH5 (Lowry et al., 2007; Taylor et al., 2007) and (1862) Apollo (Kaasalainen et al., 2007). More YORP detections should be possible in the future (e.g., Vokrouhlický et al., 2004; Scheeres et al., 2007). Finally, YORP has been suggested as a possible mechanism for the creation of binary asteroids (see, e.g., Bottke et al., 2006; Ostro et al., 2006; Scheeres et al., 2006).

Despite these achievements, the existing level of YORP theoretical modeling is still limited. So far, the YORP models described in Rubincam (2000), Vokrouhlický and Čapek (2002) and Čapek and Vokrouhlický (2004) do not rely on an exact solution of an asteroid's rotation but instead *assume* rotation occurs about the principal axis of the inertia tensor and then use a torque-averaging method. Alternative methods include Scheeres (2007), who developed a semi-analytical method that implements a linearized solution of the complete set of Euler equations about the minimum-energy state of principal axis rotation, and Nesvorný and Vokrouhlický (2007), who recently derived the first fully-analytical analysis of YORP torque components that were capable of changing the rotation rate of weakly-perturbed spheres. No group, however, has yet attempted a complete, unrestricted solution of an asteroid's rotation under the influence of YORP torques. The purpose of this paper is to explore this possibility.

In order to make our work as efficient as possible, we developed for this paper a Lie–Poisson integration scheme capable of tracking orbital and attitude motion about a center. For YORP problems, this method is at least an order of magnitude faster than conventional integrators. We checked the results of our Lie–Poisson by programming an independent integrator using traditional tools of attitude dynamics: Euler dynamical equations for angular velocity vector in the body frame and coefficients of the attitude matrix parametrized by Euler–Rodrigues parameters. This latter integrator, and related checks, are not reported in the paper. Both integrators allow us to include YORP torques and internal energy dissipation within the body.

2. Theory

2.1. Equations of motion

Attitude dynamics of rigid bodies has been considered for centuries using different approaches. In this paper we follow the early work by Euler that describes free rotation in the body's reference frame. This approach allows the dynamical (Euler–Newton) equations to be reduced to solving the evolution of the angular momentum vector in the body-fixed (BF) frame and it avoids using parameters of the transformation matrix between an inertial and BF frames such as Euler angles or quaternions. Instead, the link between the two frames of reference is obtained by tracking the BF position using vector quantities whose inertial frame position is known (either constant or using their initial values). A generalization of this approach has proved to be very useful in cases where the body's rotation is coupled to its orbital motion. This method again relegates all dynamics, including the body's orbital motion, to be uniformly described in the chosen BF frame. The theoretical basis behind our approach can be found in the works of Wang et al. (1991), Touma and Wisdom (1994) and Maciejewski (1995), though the closest predecessor is Breiter et al. (2005).

We considered the translational and rotational motion of an asteroid in orbit about a force center (the Sun). The respective masses of the asteroid and the center are m and m'. The Sun is characterized by a position vector $\mathbf{R}$ and momentum vector $\mathbf{P}$ in a BF frame of reference attached to the asteroid. The rotational motion of the asteroid is described by the angular momentum vector $\mathbf{G}$. It is both conventional and convenient to work in a BF frame defined by the principal axes of the inertia tensor $\mathbf{I}$. For that choice we have $\mathbf{I} = \mathrm{diag}(A, B, C)$ and $\mathbf{I}^{-1} = \mathrm{diag}(1/A, 1/B, 1/C)$, where $A \leqslant B \leqslant C$ are the principal values of $\mathbf{I}$. In spite of our assumption that non-rigidity effects operate on the body to dissipate its rotational energy, we neglect, for simplicity, their effects on $\mathbf{I}$ and the shape of the asteroid in the BF. This is because we assume that dissipation occurs on a microscopic level inside the body and that the amplitude of elastic flexing is negligible.

The previously listed variables would suffice to describe the problem if the asteroid and the Sun were an isolated system. However, planetary perturbations affect the orbital motion of the asteroid. We are not going to include these perturbations in full detail, but we want to include their essential character describing the asteroid's rotational motion, namely the precession of the orbital plane with respect to inertial space. This is done using the following method. We define an auxiliary vector $\mathbf{N}$, normal to the invariable plane of the planetary system, and add it to the system of dynamical variables, which now defined by a 12-dimensional vector:

$$\boldsymbol{\zeta}^{\mathrm{T}} = \left(\mathbf{R}^{\mathrm{T}}, \mathbf{P}^{\mathrm{T}}, \mathbf{G}^{\mathrm{T}}, \mathbf{N}^{\mathrm{T}}\right). \tag{1}$$

Focusing first on the non-dissipative part of the problem, we note the equations of motion derive from a Hamiltonian function

$$\mathcal{H} = \frac{\mathbf{P}^2}{2\mu} + \frac{1}{2}\mathbf{G}\cdot\mathbf{I}^{-1}\mathbf{G} + U(\mathbf{R}) - \sigma\mathbf{G}\cdot\mathbf{N}, \tag{2}$$

where $\mu = mm'/(m + m')$ and where the irrelevant kinetic energy of the Sun-body center of mass motions has been already eliminated. Because $m \ll m'$, we will use $\mu \approx m$. We shall truncate the interaction potential at the quadrupole level $U \simeq U_0(R) + U_2(\mathbf{R})$, where

$$U_0(R) = -\frac{Gmm'}{R}, \tag{3}$$

$$U_2(\mathbf{R}) = -\frac{Gm'}{R^3}\left(\mathrm{Tr}\mathbf{I} - 3R^{-2}\mathbf{R}\cdot\mathbf{I}\mathbf{R}\right) \tag{4}$$

($\mathrm{Tr}\,\mathbf{I}$ is the trace of inertia tensor $\mathbf{I}$). The novel feature here is the last term in (2), and obviously the presence of $\mathbf{N}$ among the active dynamical variables, where σ is the precession rate of the orbital plane in the inertial space. For simplicity, we assume uniform precession.

The equations of motion have a Hamiltonian form

$$\frac{\mathrm{d}\boldsymbol{\zeta}}{\mathrm{d}t} = \mathbf{J}\frac{\partial\mathcal{H}}{\partial\boldsymbol{\zeta}}, \tag{5}$$

with the Lie–Poisson structure matrix

$$\mathbf{J} = \begin{pmatrix} \mathbf{0} & \mathbf{E} & \mathbf{Q}(\mathbf{R}) & \mathbf{0} \\ -\mathbf{E} & \mathbf{0} & \mathbf{Q}(\mathbf{P}) & \mathbf{0} \\ \mathbf{Q}(\mathbf{R}) & \mathbf{Q}(\mathbf{P}) & \mathbf{Q}(\mathbf{G}) & \mathbf{Q}(\mathbf{N}) \\ \mathbf{0} & \mathbf{0} & \mathbf{Q}(\mathbf{N}) & \mathbf{0} \end{pmatrix}, \tag{6}$$

where $\mathbf{0}$ and $\mathbf{E}$ are the 3×3 zero and unit matrices, respectively. The skew-symmetric matrix $\mathbf{Q}$ associated with an arbitrary vector $\mathbf{F}$ reads

$$\mathbf{Q}(\mathbf{F}) = \begin{pmatrix} 0 & -F_3 & F_2 \\ F_3 & 0 & -F_1 \\ -F_2 & F_1 & 0 \end{pmatrix}. \tag{7}$$

Because

$$\mathbf{Q}(\mathbf{A})\mathbf{B} = \mathbf{A}\times\mathbf{B}, \tag{8}$$

it is also called the vector product matrix. Note the system (1) is not canonical, such that our variables cannot be organized into pairs of coordinates and generalized momenta, but still has structure allowing to introduce powerful tools of Lie–Poissonian mechanics (e.g., Olver, 1993). In particular, introducing a Lie–Poisson bracket $\{f, g\}$ of two arbitrary functions[2] f and g

$$\{f, g\} = \left(\frac{\partial f}{\partial\boldsymbol{\zeta}}\right)^{\mathrm{T}}\mathbf{J}\left(\frac{\partial g}{\partial\boldsymbol{\zeta}}\right), \tag{9}$$

we can rewrite the equations of motion (5) into a more straightforward Hamiltonian form

$$\frac{\mathrm{d}\boldsymbol{\zeta}}{\mathrm{d}t} = \{\boldsymbol{\zeta}, \mathcal{H}\}. \tag{10}$$

Our task below is to complement the conservative dynamics described above by additional dissipative effects that would drive long-term evolution of the system. Since our primary focus is the rotational motion of the asteroid, this means considering additional (weak) torques $\mathbf{T}$. To fold them into the right dimensionality of our approach, we define an auxiliary vector

$$\boldsymbol{\tau}^{\mathrm{T}} = \left(\mathbf{0}^{\mathrm{T}}, \mathbf{0}^{\mathrm{T}}, \mathbf{T}^{\mathrm{T}}, \mathbf{0}^{\mathrm{T}}\right), \tag{11}$$

such that the complete set of dynamical equations now reads

$$\frac{\mathrm{d}\boldsymbol{\zeta}}{\mathrm{d}t} = \{\boldsymbol{\zeta}, \mathcal{H}\} + \boldsymbol{\tau}. \tag{12}$$

[2] One directly verifies that (9) defines an antisymmetric differential operator which satisfies the Jacobi identity $\{\{f, g\}, h\} + \{\{g, h\}, f\} + \{\{h, f\}, g\} = 0$.

We discuss nature and operational definition of the appropriate dissipative torques in Section 2.3, while in the next section we briefly introduce a numerical propagator that conserves the Lie–Poisson structure (9).

2.2. Lie–Poisson algorithm for numerical propagation

Using a symplectic integration method, we split the Hamiltonian function (2) into integrable pieces. The splitting is arbitrary, but it can be advantageous if one part dominates the others and can be considered as a perturbation (e.g., McLachlan and Quispel, 2002). Recalling that our adopted BF frame of reference is that of principal axes of inertia tensor $\mathbf{I}$, we split the Hamiltonian into five parts[3]

$$\mathcal{H} = \mathcal{H}_0 + \mathcal{H}_1 + \mathcal{H}_2 + \mathcal{H}_3 + \mathcal{H}_4, \tag{13}$$

where

$$\mathcal{H}_0 = \frac{\mathbf{P}^2}{2\mu} + U_0(R) + \frac{\mathbf{G}^2}{2C}, \tag{14}$$

$$\mathcal{H}_1 = \left(\frac{1}{A} - \frac{1}{C}\right)\frac{G_1^2}{2}, \tag{15}$$

$$\mathcal{H}_2 = \left(\frac{1}{B} - \frac{1}{C}\right)\frac{G_2^2}{2}, \tag{16}$$

$$\mathcal{H}_3 = U_2(\mathbf{R}), \tag{17}$$

$$\mathcal{H}_4 = -\sigma\mathbf{G}\cdot\mathbf{N}. \tag{18}$$

In planetary applications, the G-term in $\mathcal{H}_0$ is much larger than $\mathcal{H}_1$ and $\mathcal{H}_2$, though for highly irregular asteroidal shapes this may not be true. Still, we believe that separating the G_1^2 and G_2^2 monomials as in (15) and (16) is the most efficient way to proceed. The last two pieces in (13), $\mathcal{H}_3$ and $\mathcal{H}_4$, are small perturbations.

Defining Lie derivatives L_i ($i = 0, \ldots, 4$) associated with each of the Hamiltonian terms $\mathcal{H}_i$

$$L_i f = \{f, \mathcal{H}_i\}, \tag{19}$$

we obtain a generalized second-order leapfrog map of initial state $\boldsymbol{\zeta}_0 = \boldsymbol{\zeta}(t_0)$ to final state[4] $\boldsymbol{\zeta}_1 = \boldsymbol{\zeta}(t_0 + h)$:

$$\boldsymbol{\zeta}_1 \simeq \prod_{i=0}^{4}\exp\left(\frac{h}{2}L_i\right)\prod_{i=0}^{4}\exp\left(\frac{h}{2}L_{4-i}\right)\boldsymbol{\zeta}_0. \tag{20}$$

The integration proceeds by initially choosing some value of h, which is typically of the order of minutes in our application. As in Breiter et al. (2005) we have increased the accuracy of the symplectic map using a series of leapfrog steps (20) in order to obtain a fourth-order symmetric integrator [see Yoshida, 1993, Eqs. (39) and (40)].

The exact solution of the individual patches L_0 to L_3 has been described in detail by Touma and Wisdom (1994) or

[3] We thus follow an approach of Breiter et al. (2005), who folded a "spherical top" part $G^2/(2C)$ into the unperturbed Hamiltonian piece $\mathcal{H}_0$. This is simpler than working with the symmetric top splitting of Touma and Wisdom (1994).

[4] Product here means composition of generally non-commutative operators.

Breiter et al. (2005). Here we only note that in our work we consider the L_3 (solar quadrupole) action on **G** vector, in order to describe its precession, but we neglect its action on the **P** vector [see, e.g., Touma and Wisdom, 1994, Eq. (8.0.3)]. We believe this simplification is legitimate for our analysis because it amounts to neglecting the influence of the asteroid's shape on the orbital motion of the Sun in the inertial frame. The new terms in L_4 due to $\mathcal{H}_4$ and dynamics of **N** are briefly discussed below.

While restricting to the $\mathcal{H}_4$ part of the Hamiltonian, the equations of motion (10) read

$$\frac{\mathrm{d}\mathbf{R}}{\mathrm{d}t} = -\sigma\mathbf{Q}(\mathbf{R})\mathbf{N} = -\sigma\mathbf{R}\times\mathbf{N}, \tag{21}$$

$$\frac{\mathrm{d}\mathbf{P}}{\mathrm{d}t} = -\sigma\mathbf{Q}(\mathbf{P})\mathbf{N} = -\sigma\mathbf{P}\times\mathbf{N}, \tag{22}$$

and in the same time **G** and **N** are constant. Equations (21) and (22) express regular precession of the orbital plane defined by vectors $(\mathbf{R},\mathbf{P})$ with frequency σ about **N**. The solution is easily obtained by

$$\mathbf{R}_1 = \mathbf{M}\mathbf{R}_0, \qquad \mathbf{P}_1 = \mathbf{M}\mathbf{P}_0, \tag{23}$$

where, according to the Rodrigues formula

$$\mathbf{M} = \mathbf{E} + \sin\theta\mathbf{Q}(\mathbf{N}) + 2\sin^2\frac{\theta}{2}\mathbf{Q}^2(\mathbf{N}), \tag{24}$$

and $\theta = -\sigma t$. We note $\mathcal{H}_4$ commutes with the $(R,\mathbf{P})$-dependent part of $\mathcal{H}_0$, but it does not commute with G^2. Thus it cannot be added "at no expense" to the L_0 propagator. Although some algebraic effort might yield and analytical solution for $\mathcal{H}_4 + G^2$, we prefer to keep things simple and retain the action of $\mathcal{H}_4$ as a separate step in our scheme.

In our approach, the vector **N** is considered fixed in inertial space. The fundamental variable $\boldsymbol{\zeta}$, however, contains its representation in the BF frame, where **N** moves in response to the rotation of the body. The relevant dynamics is given by Eq. (10) and reads

$$\frac{\mathrm{d}\mathbf{N}}{\mathrm{d}t} = \mathbf{N}\times\mathbf{I}^{-1}\mathbf{G}. \tag{25}$$

The evolution of **N** is decomposed similarly to the motion of **G** in the maps generated by the L_0, L_1 and L_2 operators.

2.3. Non-conservative effects

The rotation rate distribution of diameter $D \lesssim 40$ km asteroids has been previously shown to be dominated by the effects of YORP torques. We postulate that the ability to drain rotation energy from the asteroid via YORP torques could, at some point, trigger non-principal axis rotation. One of our main goals is to model this process quantitatively. Free wobbling of the **G** vector in the BF frame, however, is supposed to efficiently dissipate extra rotational energy for $D > 1$ km asteroids. As a result, any model of asteroid tumbling must also include their internal dissipation processes. The next two sections briefly outline our approach along these lines.

2.3.1. YORP torques

Thermal radiation emitted by the surface of an asteroid produced a recoil force $\mathrm{d}\mathbf{f}$ on an infinitesimal, oriented surface element $\mathrm{d}\mathbf{S}$. The total YORP torque **T** is a sum of all of these surface contributions:

$$\mathbf{T} = \int_{\mathcal{S}} \mathbf{r}\times\mathrm{d}\mathbf{f}, \tag{26}$$

where the integration is performed over the whole surface $\mathcal{S}$ of the body.[5] Assuming Lambert's emission, we have (e.g., Bottke et al., 2002)

$$\mathrm{d}\mathbf{f} = -\frac{2}{3}\frac{\varepsilon\sigma T^4}{c}\mathrm{d}\mathbf{S}, \tag{27}$$

where ε is the emissivity coefficient, σ the Stefan–Boltzmann constant, T the surface temperature and c the velocity of light.

The fundamental difficulty in determining the YORP torque is computing the correct value of T in (27) for each surface element. In general, this task requires that we solve the heat diffusion equation inside an irregular body. To avoid this complicated problem, we adopted an approximate approach and assumed the asteroid surface had zero (or near-zero) thermal conductivity. In that case, the surface temperature follows directly from energy conservation $\varepsilon\sigma T^4\,\mathrm{d}S \approx (1-A)\Phi(\mathrm{d}\mathbf{S}\cdot\mathbf{R})/R$, where Φ is the solar radiation flux impinging on the surface element $\mathrm{d}\mathbf{S}$ along direction **R** (Rubincam, 2000; Vokrouhlický and Čapek, 2002; note that when the right-hand side is negative the temperature is formally set zero). We caution the reader that our results are not applicable to very small bodies (such as meteoroids) which may have high thermal conductivities. In such a situation, this would produce nonzero lag between solar heating and the response of the surface temperature. It could even result in enough heat conducted across the body that it becomes isothermal.

By assuming zero thermal conductivity, our work implies the YORP torques depend uniquely on the (instantaneous) solar direction **R** in the BF frame of the asteroid. This allows us to pre-compute **T** for a given body on a fine grid of **R** directions and store the result in memory. In our spin–orbit history simulation for the body, we then use a three-point interpolation scheme on this grid to obtain **T** for an arbitrary **R** value.

2.3.2. Anelastic dissipation

Frictional internal processes tend to dissipate energy of the fluctuating strain field in the body (e.g., Kaula, 1968). The fluctuating strain energy is nonzero when the angular momentum vector **G** is wobbling in the BF frame. The problem of estimating the related amount of dissipated energy, which can also be considered a timescale to damp the free wobble of **G**, has been examined by several authors in the past. Unfortunately, their results differ by as much as one order of magnitude (apart from unknown material constants). We briefly discuss these results

[5] In fact, we replace integration in (26) by a summation over triangular surface facets (typically one to few thousands). Other quantities, such as volume/mass, principal values of the inertia tensor, etc. are also computed using the triangular model (e.g., Dobrovolskis, 1996).

and adopt an empirical compromise that allows us to implement dissipation effects in our simulations.

The older literature has been critically revised, and corrected in some respect, by Sharma et al. (2005) (see also Paolicchi et al., 2002). While restricting their work to the case of a spheroidal body and a commonly used Q-model of energy dissipation, these authors computed the quantities needed to evaluate the rate of change of the nutation angle θ (between $\mathbf{G}$ and the shortest or longest body axis $\mathbf{e}_z$)

$$\frac{\mathrm{d}\theta}{\mathrm{d}t} = \mp\frac{\rho a^2 \Omega_0^3}{\mu Q}\sin\theta\left(b_0 + b_2\cos^2\theta\right). \tag{28}$$

This result holds for an oblate spheroid. The upper and lower signs apply for $\theta < 90^\circ$ and $\theta > 90^\circ$, respectively; ρ is the bulk density, a the equatorial radius of the spheroid, $\Omega_0 = G/C$ is a characteristic angular velocity, μ is the rigidity and Q the (frequency-independent) quality factor.

Parameters b_0 and b_2 depend on the geometric flattening of the spheroid[6] $h = c/a \leqslant 1$:

$$b_0 = \frac{325 + 760h^2 + 608h^4 + 320h^6}{7(1+h^2)^4(13+20h^2)(15+10h^2+8h^4)}, \tag{29}$$

$$b_2 = \frac{-325 - 760h^2 + 952h^4 + 2820h^6}{7(1+h^2)^4(13+20h^2)(15+10h^2+8h^4)} + \frac{2232h^8 + 1120h^{10}}{7(1+h^2)^4(13+20h^2)(15+10h^2+8h^4)}. \tag{30}$$

The formula (28) is actually not valid for $\theta \sim 90^\circ$ for which the mathematical assumptions in the model exceed physical applicability.[7] Since the internal dissipation is assumed to conserve the total value of angular momentum G, we may write

$$\mathbf{T} = f(\mathbf{G})\mathbf{G}\times\boldsymbol{\pi}, \tag{31}$$

where

$$\boldsymbol{\pi} = \frac{\mathbf{G}\times\mathbf{e}_z}{G\sin\theta} \tag{32}$$

plays the role of an instantaneous, auxiliary axis about which the $\mathbf{G}$ vector rotates due to the dissipative effects, and

$$f(\mathbf{G}) = \mp\frac{\rho a^2}{\mu Q C^3} G\sin\theta\left(b_0 G^2 + b_2 G_z^2\right) \tag{33}$$

is the relevant rate. Sharma et al. (2005) found similar results for a prolate spheroid, where only the signs were reversed in the above equations (obviously, $h \geqslant 1$ in this case).

So far, no closed expressions for internal dissipation effects have been computed for triaxial ellipsoids, mainly because of their algebraic complexity (see, e.g., Efroimsky, 2000, 2001). In this situation, we adopt the following crude approximation. The angular momentum vector $\mathbf{G}$ circulates either about $\pm\mathbf{e}_z$ or $\pm\mathbf{e}_x$ for a freely-rotating triaxial ellipsoid (e.g., Landau and Lifschitz, 1976). When dissipation is effective, circulation about $\pm\mathbf{e}_x$ is unstable and the motion is driven toward a lower-energy wobbling near $\pm\mathbf{e}_z$. At any instant within the simulation, we can operationally define whether $\mathbf{G}$ resides in one of the two circulation zones. This is performed by computing the free-rotation energy $\mathcal{E} = \frac{1}{2}\mathbf{G}\cdot\mathbf{I}^{-1}\mathbf{G}$ and comparing it to the critical value

$$\mathcal{E}_\star = \frac{G^2}{2B}, \tag{34}$$

that separates the two rotation modes.[8]

When the $\mathbf{G}$ vector is found to circulate about $\pm\mathbf{e}_z$, we use the formulae (32) and (33) given above. Since those apply for a spheroid, we define its effective equatorial moment of inertia to be $A_\mathrm{eff} \simeq \frac{1}{2}(A+B)$, $a^2_\mathrm{eff} \simeq 2.5C/m$ and $1 + h^2_\mathrm{eff} \simeq 2A_\mathrm{eff}/C$. In the opposite case of $\mathbf{G}$ locally circulating about $\pm\mathbf{e}_x$, we use the model of a prolate spheroid but identify the long $\mathbf{e}_x$ axis as $\mathbf{e}_z$ before (thus also the nutation angle θ above is now measured from $\mathbf{e}_x$). In this case we define effective values $C_\mathrm{eff} = A$, $A_\mathrm{eff} \simeq \frac{1}{2}(C+B)$, $a^2_\mathrm{eff} \simeq 2.5A/m$ and $1 + h^2_\mathrm{eff} \simeq 2A_\mathrm{eff}/A$.

As a caveat, we should mention that our model does not correctly represent the evolution near the separatrix of the two circulation regimes, when $\mathcal{E} \simeq \mathcal{E}_\star$. This is an unavoidable feature of any such model; it is similar to the failure of a dissipation model for spheroids near nutation angle 90°. We have been experimenting with the implementation of a more complex model, where the $\mathbf{G}$ vector is driven along direction of gradient of $\mathcal{E}$ projected onto a sphere $G = \mathrm{const}$. The complexity of this approach, however, has not yet led to significantly more accurate results. For this reason, we continue to use the simplified formulation described above.

2.3.3. *Implementation to the numerical propagation*

Introducing additional (dissipative) effects in a Hamiltonian scheme such as $\boldsymbol{\tau}$ in Eq. (12) also brings with it conceptual problems, mainly by breaking its Lie–Poisson structure. Fortunately, when $\boldsymbol{\tau}$ is a small perturbation, such as the YORP effect for sufficiently large bodies, we can adopt an operational approach by introducing an additional map in the scheme expressed by Eq. (20), notably the simplest Euler-type integration

$$\boldsymbol{\zeta}_1 = \boldsymbol{\zeta}_0 + h\boldsymbol{\tau}. \tag{37}$$

We apply this step in the middle of leapfrog (20).

In the case of anelastic dissipation effects, we use the Rodrigues formula (24) to express an infinitesimal rotation of $\mathbf{G}$ about the axis $\boldsymbol{\pi}$ (replacing $\mathbf{N}$) by a small angle $f(\mathbf{G})h$. Other parameters in $\boldsymbol{\zeta}$ are conserved.

[6] We thank I. Sharma to let us know the h-dependence of the b_0 and b_2 coefficients.

[7] In particular, the period of Euler precession of $\mathbf{G}$ in the BF frame diverges for $\theta \to 90^\circ$. The model formally averages the fluctuating strain energy over this timescale and is applicable only when a dynamical timescale is much longer. At the same time, the quality factor Q, assumed to be constant, must vanish for zero frequency.

[8] For further use we also note the minimum nutation angle $\theta_\star$ of the separatrix

$$\cos^2\theta_\star = \frac{C}{B}\frac{B-A}{C-A} \tag{35}$$

and a fraction r of the circulation zone about $\pm\mathbf{e}_z$ in the $\mathbf{G}$-space:

$$r = \frac{2\theta_\star}{\pi}. \tag{36}$$

2.4. Parameter-scaling of the solutions

Parametric dependence of differential-equation solutions sometimes produce non-trivial correspondence laws that allow one to derive a solution from another known solution. This technique can be used when only numerical solutions are available, especially if solutions for some parameter values are not easy to obtain (for instance, they would require too much computer time). For this reason, we searched such rules for our fundamental system of equations, Eq. (12), that describes coupled translational-rotation motion about a center of gravity.

For a body of a given (fixed) shape we first highlight the parametric dependence of the solution $\boldsymbol{\zeta}$ on: (i) size D, (ii) bulk density ρ, (iii) internal dissipation factor μQ, (iv) precession rate σ of the orbital plane due to planetary interactions, and (v) gravitational factor Gm of the center. In addition to these parameters, we shall allow the independent time variable t to also be scaled. Here we assume we know a solution $\boldsymbol{\zeta}_1$ of the system (12) for a given set of parameters $[D_1, \rho_1, (\mu Q)_1, \sigma_1, (Gm)_1]$ and time t_1. Let now the parameters be scaled according to the following rule:

$$D_2 = \delta D_1, \tag{38}$$

$$\rho_2 = \delta^{-2(1+g)} \rho_1, \tag{39}$$

$$(\mu Q)_2 = \delta^{-2(1+g)} (\mu Q)_1, \tag{40}$$

$$\sigma_2 = \delta^g \sigma_1, \tag{41}$$

$$(Gm)_2 = \delta^{3+2g} (Gm)_1, \tag{42}$$

to obtain a new set to parameters $[D_2, \rho_2, (\mu Q)_2, \sigma_2, (Gm)_2]$. The scaling is defined using two arbitrary real parameters $\delta > 0$ and g. The solution of the system (12) that corresponds to new system of parameters reads

$$\mathbf{R}_2 = \delta \mathbf{R}_1, \tag{43}$$

$$\mathbf{P}_2 = \delta^{2-g} \mathbf{P}_1, \tag{44}$$

$$\mathbf{G}_2 = \delta^{3-g} \mathbf{G}_1, \tag{45}$$

$$\mathbf{N}_2 = \mathbf{N}_1, \tag{46}$$

and the timelike-independent variable t_2 scales as $t_2 = \delta^{-g} t_1$.

We note the scaling (38) allows us to relate solutions for bodies of different sizes as required. It also preserves a degree of internal dissipation because $\rho/(\mu Q)$ is invariant, see Eqs. (28) and (33), and for larger bodies it stretches timescale and frequencies as expected. A particular case that leaves both bulk density ρ and dissipation factor μQ invariant requires $g = -1$.

The goal of this procedure was to see whether we could speed up our integrations in some fashion by transforming spin state changes in a smaller asteroid to that of larger asteroids. Unfortunately, it appears the process is scale-invariant; roughly equal numbers of integration timesteps are needed to change a body's rotation state relative to its initial state, regardless of the body's initial size because of the above mentioned timescale stretching. Hence, the scaling law described above cannot be used to save computation time; no other scaling laws were found.

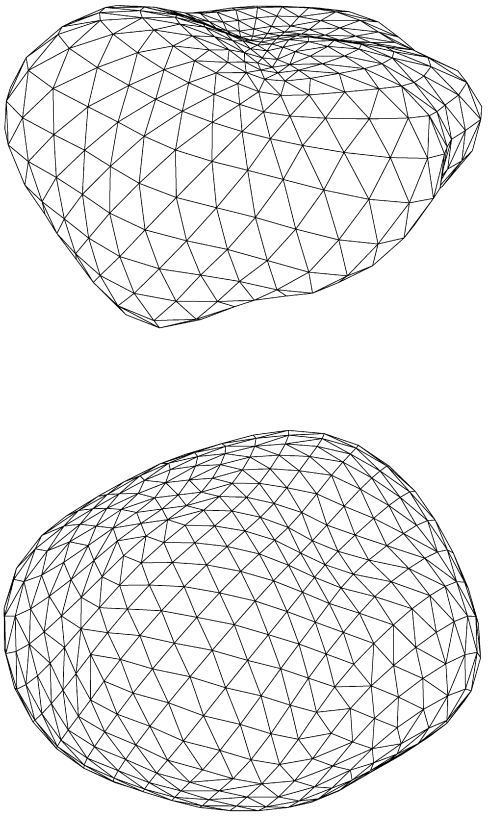

Fig. 1. Two examples of the Gaussian spheres used in our study that dynamically resemble a spheroidal body: (i) $C/B/A \simeq 1.67/1.21/1$ (top), and (ii) $C/B/A \simeq 1.35/1.10/1$ (bottom); (A, B, C) are the principal values of the inertia tensor.

3. YORP effect in full glance: numerical tests

3.1. Choice of test bodies, initial data and auxiliary algebra

In order to determine the importance of the YORP effect on small body rotation we must choose: (i) the object's shape, size and physical properties, (ii) its heliocentric orbit [i.e., which yields the initial data for $(\mathbf{R}(0), \mathbf{P}(0))$], and (iii) its initial rotation state $[\mathbf{G}(0), \mathbf{N}(0)]$. Unfortunately, the parameter space represented by these components is so large that it cannot be comprehensively analyzed with our available computer power. For this reason, we probed parameter space using the following strategy.

3.1.1. Shape

We selected 10 bodies with randomly-generated shapes using the Gaussian-sphere technique (Muinonen, 1998). The range of shapes went from oblate spheroids (for which $A \simeq B < C$; Fig. 1) to highly elongated ones (for which $A < B \simeq C$; Fig. 2). The majority were intermediate cases, described as $A < B < C$ without any particular hierarchy (Fig. 3). Animated images of all our objects can be obtained from our website http://sirrah.troja.mff.cuni.cz/~davok/. Following Vokrouhlický and Čapek (2002) we use surface triangulation to technically determine the irregular shape of the body (see also Dobrovolskis, 1996); we use 1004 surface facets of approximately equal area.

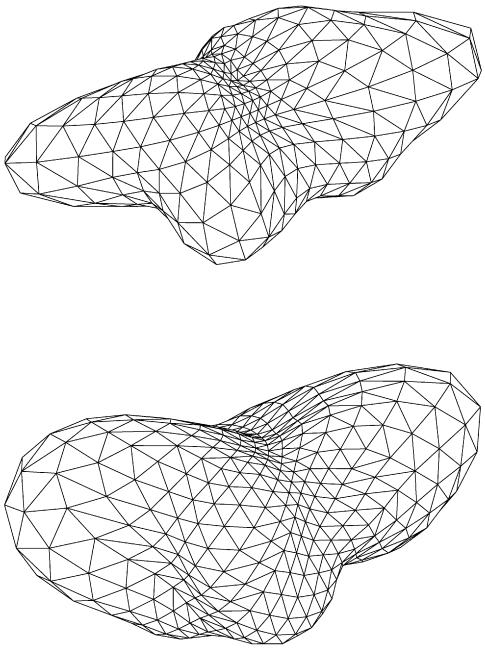

Fig. 2. Two examples of the Gaussian spheres used in our study that dynamically resemble a triaxial ellipsoid: (i) $C/B/A \simeq 3.96/3.67/1$ (top), and (ii) $C/B/A \simeq 2.91/2.66/1$ (bottom); (A, B, C) are the principal values of the inertia tensor.

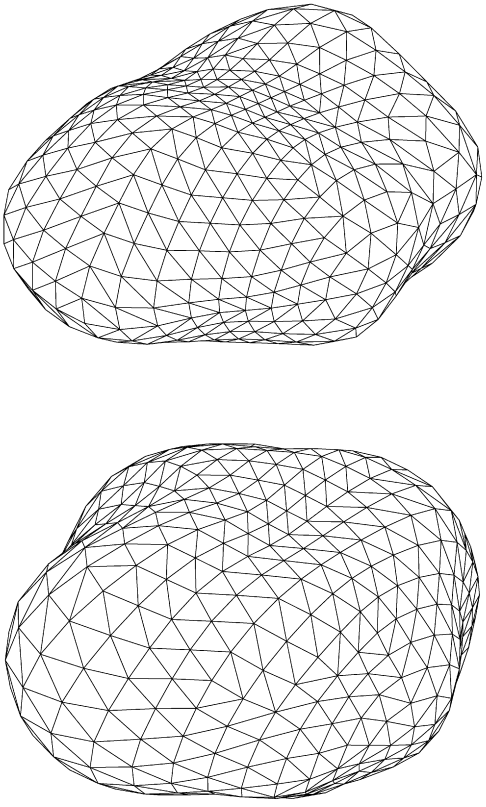

Fig. 3. Bodies 1 and 2 from Section 3.2 having a shape intermediate to dynamical spheroids or ellipsoids: (i) $C/B/A \simeq 1.75/1.45/1$ (top), and (ii) $C/B/A \simeq 1.43/1.21/1$ (bottom); (A, B, C) are the principal values of the inertia tensor.

The volume (mass), moments of inertia and other useful quantities for our arbitrary polyhedra were computed using the techniques described by Dobrovolskis (1996). Uniform scaling of vertex coordinates allowed us to create bodies with many different sizes.

The YORP torque $\mathbf{T}(\mathbf{R})$ in (26) is the net sum of torques computed for each facet of the asteroid. To save computation time in our production runs, we computed beforehand the net YORP torque for all possible solar positions (i.e., the $\mathbf{R}$ orientation in the body-fixed frame was varied). Our look-up table of YORP torques consisted of a $1^\circ \times 1^\circ$ grid of $\mathbf{R}$ directions. These values were checked during our production runs using a denser $0.1^\circ \times 0.1^\circ$ grid; we found it yielded identical results. In our simulations, we computed the YORP torques at every timestep by interpolating across these values. As mentioned above, we neglected the effects of internal energy dissipation in this paper, thus formally $\mu Q \to \infty$.

3.1.2. Heliocentric orbit

We restricted our study by only considering objects residing on circular orbits with a heliocentric distance of 2 AU. Orbital inclinations were set to 0°. As explained in Section 2, spin–orbit coupling on the orbital evolution of the body was neglected in the simulations presented below, such that we formally propagated the orbital state vector $(\mathbf{R}, \mathbf{P})$ along a fixed circular orbit with the above stated parameters. The effects of orbital plane precession were neglected in this work (thus formally $\sigma = 0$).

3.1.3. Initial rotation state

Another three degrees of freedom can be folded into specifications for the initial rotation state. Here we reduced these parameters to a simple choice: $\mathbf{N}(0) = (-1/\sqrt{2}, 0, 1/\sqrt{2})^T$ and $\mathbf{G}(0) = G(\sin\delta, 0, \cos\delta)^T$, with $G = C\omega$ and $\omega = 2\pi/(6\ \mathrm{h})$. The free parameter δ is the initial tilt of $\mathbf{G}$ vector from the principal axis $\mathbf{e}_z$ of the inertia tensor (corresponding to the SAM mode of rotation). The sensitivity of our results were tested by choosing different initial δ values (all small).

3.1.4. Auxiliary parameters

Here we introduce some auxiliary parameters. Let us denote the unit vector $\hat{\mathbf{G}} = \mathbf{G}/G$ along the direction of rotational angular momentum $\mathbf{G}$. The solution of free-top motion, a template case for the perturbed motion, can be derived from energy and angular momentum conservation and can be written in the following form (see also Whittaker, 1944; Landau and Lifschitz, 1976):

$$\hat{G}_x^2 + \hat{G}_y^2 + \hat{G}_z^2 = 1, \tag{47}$$

$$\alpha\hat{G}_x^2 + \hat{G}_y^2 + \beta\hat{G}_z^2 = p, \tag{48}$$

where $\alpha = B/A \geqslant 1$ and $\beta = B/C \leqslant 1$,

$$p = \frac{2B\mathcal{E}}{G^2} \tag{49}$$

and the $\hat{\mathbf{G}}$ components are assumed with respect to the body-fixed frame of the principal axes of the inertia tensor. Equations (47) and (48) imply $\hat{\mathbf{G}}$ evolves along the intersection of a sphere

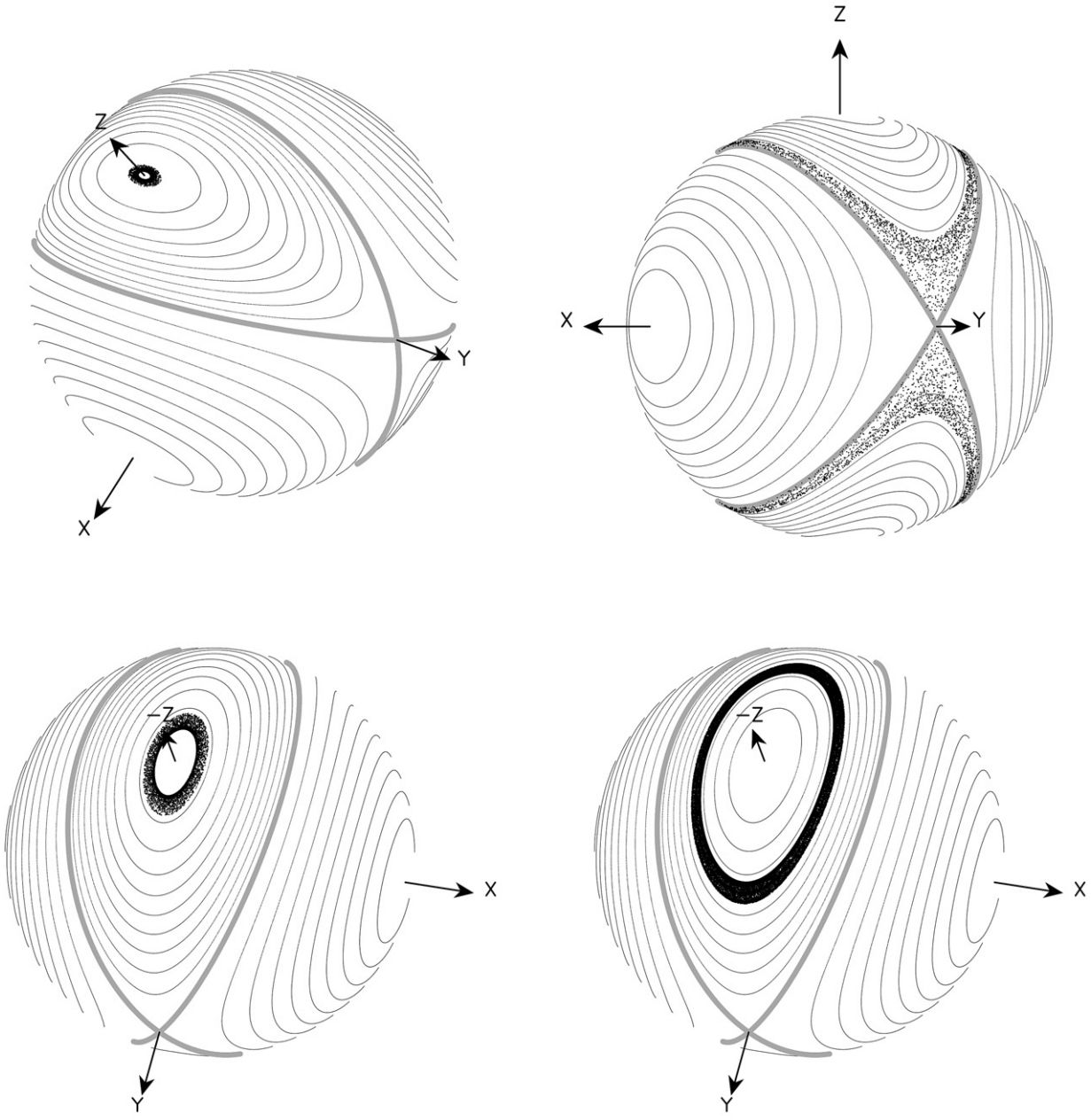

Fig. 4. Snapshots of the $\hat{\mathbf{G}}$-vector evolution in the body-fixed frame of principal axes of inertia (from top and left to bottom and right): The black dots are the direction of $\hat{\mathbf{G}}$ in equidistant timesteps in the numerical simulations. Light-gray lines are isolevels $p =$ constant from Eqs. (47) and (48); they are indicative for the free-top motion. The separatrix level $p = 1$ is shown by the thick gray line. SAM mode of rotation evolves to the small-angle circulation about $\mathbf{e}_z$ (top and left) at ∼4.3 kyr and further approaches the separatrix (top and right) at ∼4.8 kyr. At a later phase, the $\hat{\mathbf{G}}$ vector flips to the circulation zone about $-\mathbf{e}_z$; bottom left plot shows the state of minimum angular distance from $-\mathbf{e}_z$ at ∼5.5 kyr. Finally, the evolution approaches an asymptotic state shown at bottom right. The angle of view is rotated so the evolution can be better observed.

and an ellipsoid (see Fig. 4); particular solutions are parametrized by p, with values in the interval (β, α).[9] The value $p = 1$ holds for a separatrix curve between the oscillations of minimum ($\pm\mathbf{e}_z$) and maximum ($\pm\mathbf{e}_x$) energy about the stable points. The minimum value $p = \beta$ is that of the rotation about the $\pm\mathbf{e}_z$ axes (SAM mode), while the maximum value $p = \alpha$ is that of the rotation about the $\pm\mathbf{e}_x$ axes (LAM mode). In the following, we shall use the p parameter to trace the position of the $\mathbf{G}$ vector in the body-fixed frame. This is meaningful as long as the perturbations from non-conservative torques (YORP in our case) are small and lead to an adiabatic evolution of p.

3.2. General YORP evolution

To provide the reader with a sense of how things work in our YORP model, we determine below the general evolutionary paths for two selected bodies. We then discuss the dependence

[9] Our p parameter, up to a constant scaling, is related to that of Whittaker (1944, Section 70), who discusses a classical work by Poinsot describing the geometrical representation of motion of a free, triaxial top.

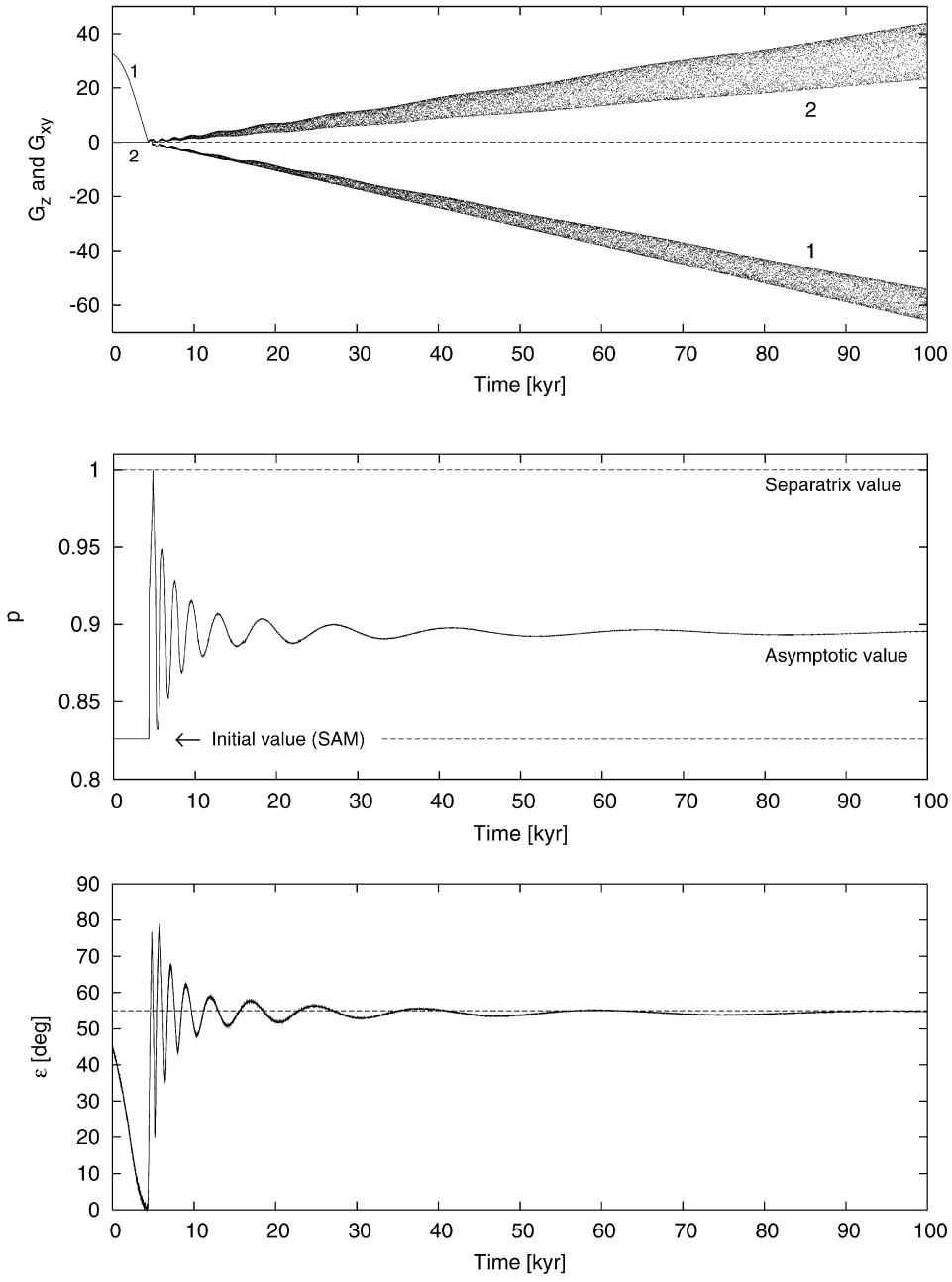

Fig. 5. Evolution from the previous figure is now shown using different variables: (top) time dependence of the G_z (curve 1) and $G_{xy} = \sqrt{G_x^2 + G_y^2}$ components (curve 2) of the angular momentum vector in the body-fixed frame; (middle) time dependence of the auxiliary parameter $p = 2B\mathcal{E}/G^2$ with $\mathcal{E} = \frac{1}{2}\mathbf{G}\cdot\mathbf{I}^{-1}\mathbf{G}$ the free rotation energy; (bottom) time dependence of the obliquity angle ε between $\mathbf{G}$ and normal $\mathbf{N}$ to the orbital plane. The initial and final phases are characterized with $p \simeq$ constant, indicating the YORP torques are a small perturbation of the free rotation. The intermediate phase is dominated by the effects of YORP torques. During the first phase (time $\leqslant 4.3$ kyr) the body rotates in the SAM mode; YORP decelerates its rotation rate and tilts the obliquity ε toward a zero value. Asymptotically, the value of ε approaches $\sim 55°$ (dashed line, bottom panel). Despite small nutation component, G increases linearly with time during the asymptotic regime.

of these results on different parameters. Our initial simulations use bodies of an equivalent size $D = 50$ m. We always start with SAM rotation (or with tumbling at very small nutation angle). YORP torques are such that they initially decelerate the rotation rate of the model asteroid.

3.2.1. *Body No. 1*

Fig. 4 shows four snapshots of the $\hat{\mathbf{G}}$-vector location in the body-fixed system during its evolution. To help the reader understand the location of its critical points, we also show isolines $p =$ constant for each frame (in this case, we have $\alpha \simeq 1.447$ and $\beta \simeq 0.826$).

The body starts in SAM rotation ($\delta = 0°$). YORP slowly decelerates the rotation rate and tilts the spin axis toward $\mathbf{N}$. Eventually, tumbling with a small nutation angle is developed (Fig. 4, top and left). Both $\mathcal{E}$ and G are decreased but in such a way that p stays approximately constant (Fig. 5). This is because at this phase YORP is merely a small perturba-

tion of the body's rotation and adiabatically conserves the p isolevel.

Eventually, there is enough energy/momentum drained out by YORP from the body's rotation motion that YORP ceases to be a small perturbation and the adiabaticity of the body's evolution is violated. The $\hat{\mathbf{G}}$ vector drifts away from the $\mathbf{e}_z$ axis and reaches the separatrix zone about two possible types of free-top circulation (Fig. 4, top and right). In the presence of perturbations, the evolution near the separatrix is chaotic and predictable only in a probabilistic manner. In our case, the $\hat{\mathbf{G}}$ vector passes through the circulation zone to near $-\mathbf{e}_z$ (Fig. 4, bottom and left). Finally, though, YORP forces the $\hat{\mathbf{G}}$ vector to circulate about $-\mathbf{e}_z$ at a larger relative angle of $\sim 30°$ (Fig. 4, bottom and right), while G steadily increases. It should be mentioned that the formal quantity $2\pi/\omega$ never exceeds ~ 740 h during the evolution.

At the final stage of evolution, YORP again becomes a perturbation effect to the body's free rotational motion and $\mathcal{E}$ increases such that the asymptotic evolution is again characterized by $p =$ constant (Fig. 5). We also note that during this phase, $\mathrm{d}G/\mathrm{d}t = \hat{\mathbf{G}} \cdot \mathbf{T} =$ constant. The new asymptotic state of tumbling has the following properties: (i) unlike deceleration in the simplified case, the rotation gains energy by the YORP torques in an unlimited way, (ii) the $\hat{\mathbf{G}}$ vector freezes in inertial space, since the rotation becomes asymptotically close to resembling a free-top along a direction that, on average, is tilted away from the orbital plane. In our case, this asymptotic tilt angle is $\sim 55°$ (Fig. 5). While the exact value depends on the chosen body, we note below that its value, rather remarkably, is clustered about this typical value. We can only speculate that this feature has a similar or related origin to that of non-tumbling bodies (see, e.g., Vokrouhlický et al., 2003; Nesvorný and Vokrouhlický, 2007).

The above integration was repeated, except this time we started things with a small initial tumbling component. In particular, we took $\delta = 0.1°$ and $\delta = 1°$ (the initial tilt of $\mathbf{G}$ from $\mathbf{e}_z$). Fig. 6 shows the evolution of p in these simulations. We note the onset of tumbling is facilitated by the initial component, such that with $\delta = 1°$, p deviates from the initial SAM value described above. While their evolutionary paths are different, these three simulations happen to be directed toward the same asymptotic state. However, since the evolution near the separatrix is chaotic, we cannot yet state that the observed asymptotic evolution is the common attractor of all possible cases. Indeed, in a number of simulations below, we found that initial data only nominally different from the cases above evolved toward different asymptotic states, even while sharing all of the properties listed above.

3.2.2. *Body No. 2*

In some cases, the asymptotic state is preceded by a more complicated evolution than indicated in the simple example above. This means the $\hat{\mathbf{G}}$ vector may chaotically wander for a longer period of time, visiting different circulation zones about $\pm\mathbf{e}_z$ and/or $\pm\mathbf{e}_x$, before being directed toward the asymptotic track. Fig. 7 shows such a case. The asymptotic state is represented here by circulation about the $\mathbf{e}_x$ direction of LAM

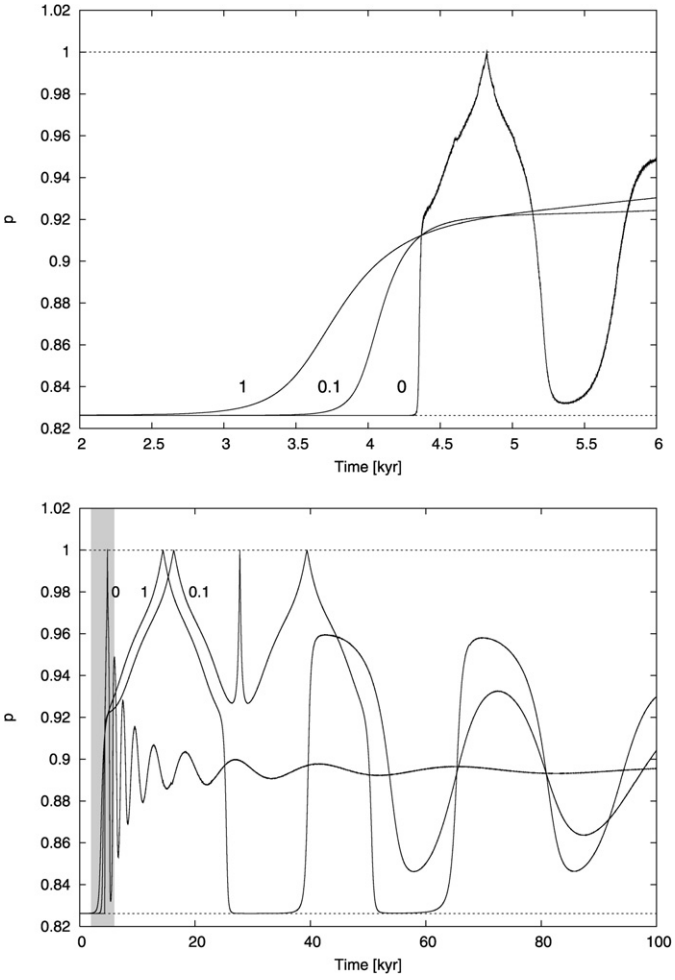

Fig. 6. Evolution of the p parameter for the body from Figs. 4 and 5, but now for three different initial tilt angles δ between $\mathbf{e}_z$ and $\mathbf{G}$: (i) $\delta = 0°$, (ii) $\delta = 0.1°$, and (iii) $\delta = 1°$. Top panel is a zoom of the initial phase (shown as a dashed interval in the bottom panel).

rotation. Interestingly, though, the asymptotic obliquity value (tilt of $\mathbf{G}$ from $\mathbf{N}$) moves once again to $\sim 55°$.

An interesting segment of evolution was denoted by a shaded rectangle in Fig. 7. During this period of time the $\mathbf{G}$ vector seems to adhere a periodic solution since its orientation was repeatedly flipping in between the tumbling zones around $\mathbf{e}_z$ and $-\mathbf{e}_z$. The solution finally diverged from this cycle indicating probably that such a periodic solution is unstable.

Fig. 8 indicates that analogous stable cycles of YORP evolution also exist. Here we started our simulation of body No. 2 with an initial $1°$ tilt between the $\mathbf{G}$ and $\mathbf{e}_z$ vectors. During our integration, the $\mathbf{G}$ vector periodically flipped between $\mathbf{e}_z$ and $-\mathbf{e}_z$ orientations in the body-frame, with the separatrix quickly crossed in each case.

3.2.3. *Comments on additional simulations*

We ran simulations similar to those presented above for 8 other Gaussian spheres. The results share the same pattern: (i) the initial SAM rotation becomes destabilized by YORP torques when the rotation rate is long enough, (ii) an asymptotic state emerges from the irregular tumbling that is characterized

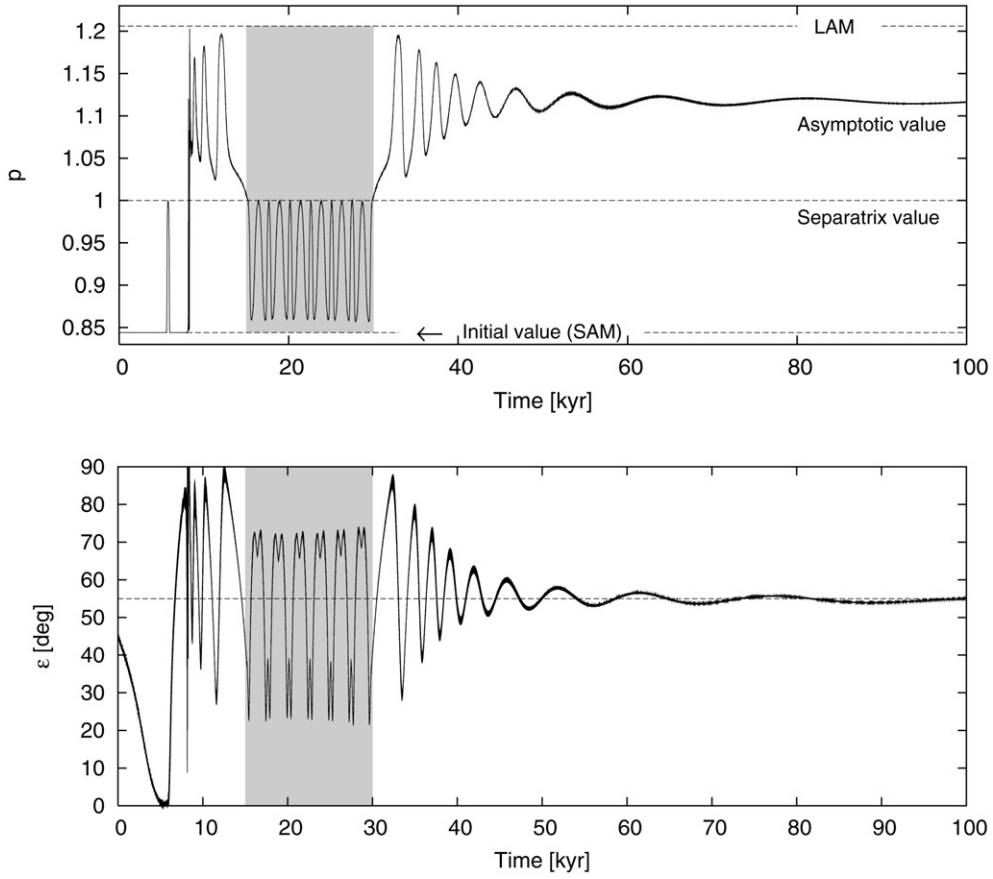

Fig. 7. Evolution of spin parameters for the second test body: (top) time dependence of the auxiliary parameter $p = 2B\mathcal{E}/G^2$ with $\mathcal{E} = \frac{1}{2}\mathbf{G}\cdot\mathbf{I}^{-1}\mathbf{G}$ the free-rotation energy; (bottom) time dependence of the obliquity angle ε between $\mathbf{G}$ and normal $\mathbf{N}$ to the orbital plane. The initial and final phases are characterized with $p \simeq$ constant, indicating the YORP torques are a small perturbation of the free rotation. The body initially rotates in the SAM mode, while asymptotically tumbles in the LAM rotation zone at roughly constant angle from $\mathbf{e}_x$. During the intermediate phase, the body visits different SAM and LAM zones. For 15 kyr (shaded interval) the evolution seems to adhere an unstable periodic solution. The obliquity asymptotically evolves toward the $\sim 55°$ value (dashed curve).

by circulation of the $\mathbf{G}$ vector about $\pm\mathbf{e}_z$ or $\pm\mathbf{e}_x$ with linearly increasing magnitude G (in a minority of cases the solution adheres to a stable periodic solution such as in the last example above; Fig. 8), (iii) the inertial space orientation of $\mathbf{G}$ is such that its tilt to $\mathbf{N}$ is close to either 55° or 125°. For the $D = 50$ m bodies in our sample, the median time to reach the onset of macroscopic tumbling was 5.3 kyr.

We also reran these simulation for bodies of equivalent size of 200 m. The qualitative features of the evolution remained the same, but the timescale was rescaled by a factor 16, suggesting it is proportional to the size as $\propto D^2$. This behavior will be explained in the next section.

4. Analytical model for origin of tumbling

No complete analytical theory describing how YORP torques influence the rotation of an arbitrarily-shaped body has yet been published. It is not even clear if such a theory is possible, considering how despun objects undergo chaotic tumbling. A recent analysis by Scheeres (2007) is based upon a somewhat restrictive assumption that the spin vector does not deviate significantly from the maximum inertia axis. For this reason, it cannot predict the tumbling reported in this paper. On the other hand, we do not expect from an analytical model more than a qualitative explanation of the physical mechanism and a hint of its dependence on physical parameters and initial conditions.

Intuitively, there are two sources of large-scale, long-term phenomena in a dynamical system: (i) a resonance, or (ii) a constant term in the right-hand side of a body's equations of motion. Although the former is practically inevitable in the case of a systematic slowdown of a body's rotation, we focus here on the latter case that should act on all initial rotation states. If we identify some constant components of the YORP torques, which result from averaging the torques over all solar orientations in the body-fixed frame, we obtain a problem that is well known in spacecraft attitude dynamics, namely that of a *rigid body with self-excitation*. The response of the angular momentum vector to a constant thrust exerted by rocket engines has been studied in a number of papers (see, e.g., Tsiotras and Longuski, 1991; Livneh and Wie, 1997; Tong and Tabarrok, 1997; Gick et al., 2000; Longuski et al., 2005) mostly by means of perturbation methods; the only case that can be solved exactly is that of a body with rotational symmetry.

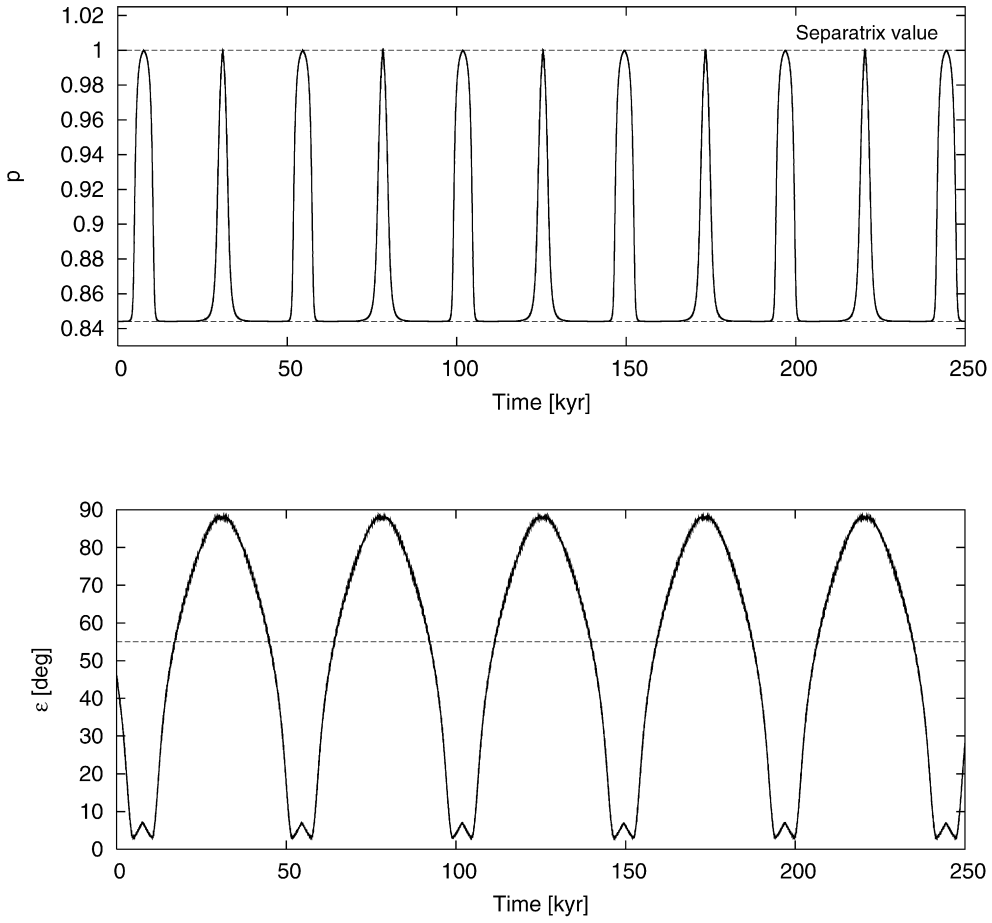

Fig. 8. Evolution of spin parameters for the second test body with an initial tilt of 1° between $\mathbf{G}$ and $\mathbf{e}_z$ vectors: (top) time dependence of the auxiliary parameter $p = 2B\mathcal{E}/G^2$ with $\mathcal{E} = \frac{1}{2}\mathbf{G}\cdot\mathbf{I}^{-1}\mathbf{G}$ the free-rotation energy; (bottom) time dependence of the obliquity angle ε between $\mathbf{G}$ and normal $\mathbf{N}$ to the orbital plane. As long as we tracked the body's evolution, it adhered to a periodic solution characterized by rotation about the principal axes $\pm\mathbf{e}_z$ with excursions toward the separatrix mode when it entered a tumbling state. The obliquity avoids settling near the ∼55° value (dashed curve) but oscillates about it; during its decreasing phase the body rotates about $\mathbf{e}_z$, while during the increasing phase the body rotates about $-\mathbf{e}_z$.

Thus, consider a toy model of the Euler equations

$$\frac{\mathrm{d}\boldsymbol{G}}{\mathrm{d}t} = \boldsymbol{G}\times\mathbf{I}^{-1}\boldsymbol{G} + \overline{\boldsymbol{T}}, \tag{50}$$

with a constant torque $\overline{\boldsymbol{T}} = (T_1, T_2, T_3)^{\mathrm{T}} \neq \mathbf{0}$. In this paper, we also assume that $T_1T_2T_3 \neq 0$. In a sequence of papers, Longuski, Tsiotras and collaborators developed an approximate solution of Eq. (50) using

$$G_3(t) = G_3(0) + T_3 t, \tag{51}$$

as the first approximation and then solving the remaining two equations for G_1, G_2 that form a linear system with time-dependent coefficients. Tsiotras and Longuski (1991) justify Eq. (51) as a result of neglecting the triaxiality of the body, but—interestingly—the same result is valid even for a significantly triaxial shape, provided G_3 is understood as the mean variable in the context of the first-order averaging method.

Rearranging the approximate solution provided in Tsiotras and Longuski (1991), we introduce a complex variable

$$\Gamma = G_1\sqrt{(C-A)B} + iG_2\sqrt{(C-B)A}, \tag{52}$$

which evolves according to

$$\Gamma(t) = e^{i\xi(t)}\big(\Gamma(0)e^{-i\xi(0)} + FI_\omega(t)\big), \tag{53}$$

where

$$\begin{aligned}
F &= T_1\sqrt{(C-A)B} + iT_2\sqrt{(C-B)A},\\
I_\omega(t) &= \frac{\sqrt{\pi C}\big(s(t)E(|\xi(t)|) - s(0)E(|\xi(0)|)\big)}{\sqrt{|T_3|\sigma}},\\
\xi(t) &= \frac{\sigma G_3^2(t)}{2CT_3},\\
\sigma &= \sqrt{\frac{(C-A)(C-B)}{AB}},\\
s(t) &= \operatorname{sgn}\big(G_3(t)\big)\operatorname{sgn}(T_3),\\
E(x) &= \frac{1}{\sqrt{2\pi}}\int_0^x \frac{\mathrm{d}q}{\sqrt{q}}\exp\big(-i\operatorname{sgn}(T_3)q\big)\\
&= C_2(x) - i\operatorname{sgn}(T_3)S_2(x).
\end{aligned} \tag{54}$$

Functions C_2 and S_2 are modified Fresnel sine and cosine integrals (e.g., Abramowitz and Stegun, 1964, Chap. 7.3). In further

discussion we will use asymptotic expansions

$$C_2(x) \approx \frac{1}{2} + \frac{\sin x}{\sqrt{2\pi x}} + O\left(x^{-3/2}\right), \tag{55}$$

$$S_2(x) \approx \frac{1}{2} - \frac{\cos x}{\sqrt{2\pi x}} + O\left(x^{-3/2}\right) \tag{56}$$

valid for $x \gg 1$.

The Tsiotras–Longuski (TL) theory has to be used with caution, because it is inherently restricted to the rotation mode with $p < 1$ (SAM). It is straightforward exercise to derive its $p > 1$ (LAM) complement, but none of the solutions is capable of following a sudden transition from one mode to another, a possibility that may happen in the constant torque problem. Thus, a realistic application of TL theory consists of using it only until the $p \sim 1$ separatrix is reached or until after it is left by the $\boldsymbol{G}$ vector.

Let us now see how the TL approximate analytic solution above may help us understand some of our numerical results from Section 3.2. Suppose the initial value of $\boldsymbol{G}(0)$ is such that $G_3(0) > 0$ and $p < 1$. According to the TL theory, there are two possible scenarios in this case, depending on the sign of T_3:

1. If $T_3 > 0$, the G_3 component grows linearly, whereas G_1 and G_2 oscillate around some guiding centers. As $t \to \infty$, the guiding centers approach 0 and the oscillation amplitudes shrink to finite, nonzero values A_1 for G_1, and A_2 for G_2, such that

$$A_1^2 = G_1^2(0) + \frac{A}{C-A}\left[\frac{C-B}{B}G_2^2(0) + \frac{2C}{G_3(0)}\left(G_2(0)T_1 - G_1(0)T_2 + \frac{C}{2G_3(0)}\left(\frac{BT_1^2}{C-B} + \frac{AT_2^2}{C-A}\right)\right)\right],$$

$$A_2 = A_1\sqrt{\frac{B(C-A)}{A(C-B)}}. \tag{57}$$

   In other words, the projection of $\boldsymbol{G}$ onto the G_1, G_2 plane tends to an ellipse centered at the origin.
   Of course, the unbounded growth of G_3 leads asymptotically to the final state $\boldsymbol{G} = (0, 0, 1)^{\mathrm{T}}$, regardless of the final nonzero values of G_1 and G_2.
2. If $T_3 < 0$, the third component of $\boldsymbol{G}$ decreases linearly, reaching the value $G_3 = 0$ after the time

$$\Delta t = -\frac{G_3(0)}{T_3}. \tag{58}$$

   This elementary but very useful formula derived from Eq. (51) estimates the time required to enter the tumbling mode. Note that if $T_3 < 0$, even the initial state $\boldsymbol{G}(0) = \boldsymbol{e}_z$ is unstable and moves $\boldsymbol{G}$ towards the separatrix. On its way, Eq. (53) indicates that the G_1 and G_2 components oscillate with an increasing amplitude.

In order to test our analytic formulae, we output values of the YORP torques during the numerical evolutions reported in Section 3.2 Passing these values through a Fourier filter on a running-box window, we verified that all three components (T_1, T_2, T_3) have nonzero mean values (this is a somewhat trivial conclusion as far as the third component T_3 is concerned, because its nonzero mean value is responsible for the YORP acceleration or deceleration of the rotation rate already recognized by Rubincam, 2000). Here we compared the estimated timescale Δt from Eq. (58) to acquire a tumbling rotation state with our numerically-determined timescale and found the two values were is good agreement. Note that because $\Delta t \propto D^2$ (Rubincam, 2000; Vokrouhlický and Čapek, 2002), the timescale to the onset of tumbling scales with the size of the body used in our numerical experiments.

After reaching the separatrix, the evolution of $\boldsymbol{G}$ either continues as precession around $\boldsymbol{e}_z$ (with $G_3 < 0$) and the TL theory still applies, or precession around $\boldsymbol{e}_x$ occurs and a modification of the theory is required with T_1 and G_1 taking the roles of T_3 and G_3. A qualitative description of the latter case is similar to the $p < 1$ case discussed above.

Even elementary considerations lead us to the conclusion that, if $|G_3|$ experiences unlimited growth, the energy value tends to $\mathcal{E} \approx G_3^2/(2C)$, and the square of total momentum tends to $G^2 \approx G_3^2$. This means the value of p should converge to $p \approx B/C = \beta$. In the second evolution variant, when $|G_1|$ grows and $\boldsymbol{G}$ tends to $\pm\boldsymbol{e}_x$, the quantity p converges to $p \approx B/A = \alpha$. As a result, the simple constant-torque model described above cannot explain the new asymptotic states determined by the numerical experiments from Section 3.2. An appropriate analytic model that would allow their description is beyond the scope of this paper.

5. Conclusions

In this paper, we extended our knowledge of YORP asymptotic states using a more complete model than has been used before. We have shown that the previously-determined states of infinitely slow rotation rate, or sun-synchronous if solar torques were included, do not persist and instead lead to the onset of tumbling rotation states. Using a simple analytical model, we explained why tumbling is excited by YORP.

We caution that at this stage of analysis, the timescales to determine the onset of tumbling by YORP, and particularly the asymptotic states, are mathematical results. The question of whether they exist in reality or not should be studied using a more complete and sophisticated approach. For instance, very small bodies with $D \lesssim 50$ m are unlikely to have an insulating cover of regolith; this means their surfaces may be characterized by exposed rock with high thermal conductivity values. This would violate the zero thermal conductivity cases examined here. Accordingly, our results may not be applicable to meter-sized meteoroids (to learn more about the role of the surface conductivity on the YORP effect, see, Čapek and Vokrouhlický, 2004).

It is also important to note that the effects of internal dissipation within multi-kilometer asteroids present an obstacle for the efficient onset of tumbling by YORP over a timescale limited by collisional powerful enough to affect their spin states.

Efficient internal dissipation processes would damp the asymptotic tumbling states, reported in this paper, to SAM rotation because of steadily-increasing rotational energy (Section 3). In such a scenario, tumbling states would only be temporary excursions between SAM rotation modes. A detailed analysis of such effects is beyond the scope of this paper.

Using asteroid lightcurves, Pravec et al. (2005) searched for bodies that could be in an excited, non-principal-axis rotation state. According to their work, these objects are located below a critical line ℓ_1 in a plot of ω vs D, where damping of the excitation by internal dissipation would either take longer than ~4 Gyr or the body's estimated collisional lifetime. If we now compare the order-of-magnitude estimate of the timescale needed for YORP to push a body from a SAM state into a tumbling state to the dissipation timescale in Harris (1994), we find that below $(D/P)^2 \sim \kappa/a$ line (ℓ_2), YORP should win over dissipation damping to push an asteroid's rotation into an excited rotation state. Here $\kappa \sim (0.1–0.5)$ if D is in kilometers, rotation period P in hours and semimajor axis a in astronomical units. The critical line ℓ_2, if plotted on an ω vs D plot, would—for nominal parameter values—lie above ℓ_1, which would make the parametric space where tumbling asteroids are expected even larger.

Curiously, a number of apparently SAM-rotating $D \sim (0.1–5)$ km asteroids reside below the ℓ_1 and ℓ_2 critical lines in the ω vs D plot (A. Harris, personal communication). Rotating very slowly for their size, these objects cannot damp their excitation energy within their collisional lifetimes and thus should be easy targets for YORP to quickly establish tumbling. Their existence is a true mystery.

Acknowledgments

This work has been partly supported by the Grant Agency of the Czech Republic (Grant 205/05/2737), the Research Program MSM0021620860 of the Czech Ministry of Education and by the Polish State Committee of Scientific Research Grant 1 P03D 020 27. The work of D.N. and W.F.B. was supported by NASA's Planetary, Geology and Geophysics program. We thank Alan Harris (SSI) and Dan Scheeres who, as referees, helped to improve the first version of this paper.

References

Abramowitz, M., Stegun, I., 1964. Handbook of Mathematical Functions. National Bureau of Standards, Washington.

Bottke, W.F., Vokrouhlický, D., Rubincam, D.P., Brož, M., 2002. Dynamical evolution of asteroids and meteoroids using the Yarkovsky effect. In: Bottke, W.F., Cellino, A., Paolicchi, P., Binzel, R.P. (Eds.), Asteroids III. Univ. of Arizona Press, Tucson, pp. 395–408.

Bottke, W.F., Vokrouhlický, D., Rubincam, D.P., Nesvorný, D., 2006. The Yarkovsky and YORP effects: Implications for asteroid dynamics. Annu. Rev. Earth Planet. Sci. 34, 157–191.

Breiter, S., Melendo, B., Bartczak, P., Wytrzyszczak, I., 2005. Synchronous motion in the Kinoshita problem. Application to satellites and binary asteroids. Astron. Astrophys. 437, 753–764.

Burns, J.A., Lamy, P.L., Soter, S., 1979. Radiation forces on small particles in the Solar System. Icarus 40, 1–48.

Čapek, D., Vokrouhlický, D., 2004. The YORP effect with finite thermal conductivity. Icarus 172, 526–536.

Dobrovolskis, A.R., 1996. Inertia of any polyhedron. Icarus 124, 698–704.

Ďurech, J., Scheirich, P., Kaasalainen, M., Grav, T., Jedicke, R., Denneau, L., 2007. Physical models of asteroids from sparse photometric data. In: Milani, A., Valsecchi, G.B., Vokrouhlický, D. (Eds.), Near Earth Objects, Our Celestial Neighbors: Opportunity and Risk. Cambridge Univ. Press, Cambridge, pp. 191–200.

Efroimsky, M., 2000. Precession of a freely rotating rigid body. Inelastic relaxation in the vicinity of poles. J. Math. Phys. 41, 1854–1888.

Efroimsky, M., 2001. Relaxation of wobbling asteroids and comets—Theoretical problems, perspectives of experimental observation. Planet. Space Sci. 49, 937–955.

Gick, A., Williams, M.H., Longuski, J.M., 2000. Periodic solutions for spinning asymmetric rigid bodies with constant principal-axis torque. J. Guidance Control Dynam. 23, 781–788.

Harris, A.W., 1994. Tumbling asteroids. Icarus 107, 209–211.

Kaasalainen, M., Ďurech, J., Warner, B.D., Krugly, Y.N., Gaftonyuk, N., 2007. Direct detection of acceleration in Asteroid (1862) Apollo's rotation due to radiation torques. Nature 446, 420–422.

Kaula, W.M., 1968. An Introduction to Planetary Physics. The Terrestrial Planets. Wiley & Sons, New York.

Landau, L.D., Lifschitz, E.M., 1976. Mechanics. Pergamon Press, Oxford.

Livneh, R., Wie, B., 1997. New results for an asymmetric rigid body with constant body-fixed torques. J. Guidance Control Dynam. 20, 873–881.

Longuski, J.M., Gick, R.A., Ayoubi, M.A., Randall, L., 2005. Analytical solutions for thrusting, spinning spacecraft subject to constant forces. J. Guidance Control Dynam. 28, 1301–1308.

Lowry, S., and 9 colleagues, 2007. Direct observational detection of the asteroidal YORP effect. Science 316, 272–274.

Maciejewski, A.J., 1995. Reduction, relative equilibria and potential in the two rigid bodies problem. Celest. Mech. Dynam. Astron. 63, 1–28.

McLachlan, R.I., Quispel, G.R.W., 2002. Splitting methods. Acta Numer. 11, 341–434.

Morbidelli, A., Vokrouhlický, D., 2003. The Yarkovsky-driven origin of near-Earth asteroids. Icarus 163, 120–134.

Muinonen, K., 1998. Introducing the Gaussian shape hypothesis for asteroids and comets. Astron. Astrophys. 332, 1087–1098.

Nesvorný, D., Vokrouhlický, D., 2007. Analytic theory of the YORP effect for near-spherical objects. Astron. J., in press.

Olver, P.J., 1993. Application of Lie groups to differential equations. In: Axler, S., Gehring, F.W., Ribet, K.A. (Eds.), Graduate Texts in Mathematics, vol. 107. Springer, New York, pp. 378–421.

Ostro, S.J., Hudson, R.S., Benner, L.A.M., Giorgini, J.D., Margi, C., Margot, J.-L., Nolan, M.C., 2002. Asteroid radar astronomy. In: Bottke, W.F., Cellino, A., Paolicchi, P., Binzel, R.P. (Eds.), Asteroids III. Univ. of Arizona Press, Tucson, pp. 151–168.

Ostro, S.J., and 15 colleagues, 2006. Radar imaging of binary near-Earth Asteroid (66391) 1999 KW4. Science 314, 1276–1280.

Paolicchi, P., Burns, J.A., Weidenschilling, S.J., 2002. Side effects of collisions: Spin rate changes, tumbling rotation states, and binary asteroids. In: Bottke, W.F., Cellino, A., Paolicchi, P., Binzel, R.P. (Eds.), Asteroids III. Univ. of Arizona Press, Tucson, pp. 517–526.

Pravec, P., and 19 colleagues, 2005. Tumbling asteroids. Icarus 173, 108–131.

Pravec, P., Harris, A.W., Warner, B.D., 2007. NEA rotations and binaries. In: Milani, A., Valsecchi, G.B., Vokrouhlický, D. (Eds.), Near Earth Objects, Our Celestial Neighbors: Opportunity and Risk. Cambridge Univ. Press, Cambridge, pp. 167–176.

Rubincam, D.P., 2000. Radiative spin-up and spin-down of small asteroids. Icarus 148, 2–11.

Scheeres, D.J., 2007. The dynamical evolution of uniformly rotating asteroids subject to YORP. Icarus 188, 430–450.

Scheeres, D.J., and 15 colleagues, 2006. Dynamical configuration of binary near-Earth Asteroid (66391) 1999 KW4. Science 314, 1280–1283.

Scheeres, D.J., Abe, M., Yoshikawa, M., Nakamura, R., Gaskell, R.W., Abell, P.A., 2007. The effect of YORP on Itokawa. Icarus 188, 425–429.

Sharma, I., Burns, J.A., Hui, C.-Y., 2005. Nutational damping times in solids of revolution. Mon. Not. R. Astron. Soc. 359, 79–92.

Slivan, S.M., 2002. Spin vector alignment of Koronis family asteroids. Nature 419, 49–51.

Slivan, S.M., Binzel, R.P., Crespo da Silva, M., Kaasalainen, L.D., Lyndaker, M.M., Krčo, M., 2003. Spin vectors in the Koronis family: Comprehensive results from two independent analyses of 213 rotation lightcurves. Icarus 162, 285–307.

Taylor, P., and 11 colleagues, 2007. Increasing spin rate of Asteroid 54509 (2000 PH5) a result of the YORP effect. Science 316, 274–277.

Tong, X., Tabarrok, B., 1997. Bifurcation of self-excited rigid bodies subjected to small perturbation torques. J. Guidance Control Dynam. 20, 123–128.

Touma, J., Wisdom, J., 1994. Lie–Poissonian integrators for rigid body dynamics in the Solar System. Astron. J. 107, 1189–1202.

Tsiotras, P., Longuski, J.M., 1991. A complex analytic solution for the attitude motion of a near-symmetric rigid body under body-fixed torques. Celest. Mech. Dynam. Astron. 51, 281–301.

Vokrouhlický, D., Čapek, D., 2002. YORP-induced long-term evolution of the spin state of small asteroids and meteoroids. Rubincam's approximation. Icarus 159, 449–467.

Vokrouhlický, D., Nesvorný, D., Bottke, W.F., 2003. The vector alignments of asteroid spins by thermal torques. Nature 425, 147–152.

Vokrouhlický, D., Čapek, D., Kaasalainen, M., Ostro, S.J., 2004. Detectability of YORP rotational slowing of Asteroid 25143 Itokawa. Astron. Astrophys. 414, L21–L24.

Vokrouhlický, D., Brož, M., Bottke, W.F., Nesvorný, D., Morbidelli, A., 2006a. Yarkovsky/YORP chronology of asteroid families. Icarus 182, 111–142.

Vokrouhlický, D., Brož, M., Bottke, W.F., Nesvorný, D., Morbidelli, A., 2006b. The peculiar case of the Agnia asteroid family. Icarus 183, 349–361.

Wang, L.-S., Krishnaprasad, P.S., Maddocks, J.H., 1991. Hamiltonian dynamics of a rigid body in a central gravitational field. Celest. Mech. Dynam. Astron. 50, 349–386.

Whittaker, E.T., 1944. A Treatise on the Analytical Dynamics of Particles and Rigid Bodies. Dover Publications, New York.

Yoshida, H., 1993. Recent progress in the theory and application of symplectic integrators. Celest. Mech. Dynam. Astron. 56, 27–43.